Prospective high thermoelectric performance of the heavily p-doped half-Heusler compound CoVSn

Hongliang Shi, Wenmei Ming, David S. Parker, Mao-Hua Du, and David J. Singh

Potential high thermoelectric performance of heavily p-doped half-heusler CoVSn

Hongliang Shi[1], Wenmei Ming[2], David S. Parker[2], Mao-Hua Du[2], and David J. Singh[3]

[1]*Key Laboratory of Micro-Nano Measurement-Manipulation and Physics (Ministry of Education),*
Department of Physics, Beihang University, Beijing 100191, China
[2]*Materials Science & Technology Division, Oak Ridge National Laboratory, Oak Ridge, Tennessee 37831, USA and*
[3]*Department of Physics and Astronomy, University of Missouri, Columbia, Missouri 65211-7010, USA*
(Dated: April 17, 2017)

The electronic structure and transport properties of half-heusler compound CoVSn are systematically studied by combining first-principles electronic structure calculations and Boltzmann transport theory. The band structure at the valence band edge is complex with multiple maxima derived from hybridized transition element d states. The result is a calculated thermopower larger than 200 μV/K within a wide range of doping concentration and temperatures for heavily doped p-type CoVSn. The thermoelectric properties additionally benefit from the corrugated shapes of the hole pockets in our calculated isoenergy surfaces. Our calculated power factor $S^2\sigma/\tau$ (with respect to an average unknown scattering time) of CoVSn is comparable to that of FeNbSb. A smaller lattice thermal conductivity can be expected from the smaller group velocities of acoustical modes compared to FeNbSb. Overall, good thermoelectric performance for CoVSn can be expected by considering the electronic transport and lattice thermal conductivity.

PACS numbers: Computational Physics, Condensed Matter Physics

I. INTRODUCTION

Thermoelectric devices can directly convert thermal to electrical energy and have many applications such as refrigeration and power generation through waste-heat recovery. The performance of a thermoelectric material is characterized by a dimensionless figure of merit ZT by the following expression:

$$ZT = \frac{S^2\sigma T}{\kappa_e + \kappa_l}. \tag{1}$$

Here, S is the Seebeck coefficient or thermopower, σ is the electrical conductivity, T is the absolute temperature, κ_e is the electronic thermal conductivity, and κ_l is the lattice thermal conductivity. Seebeck coefficient is decreased as the carrier concentration n is increased, while σ behaves in the opposite way. Therefore, in order to get high power factor ($S^2\sigma$), there is the compromise between large Seebeck coefficient and high electrical conductivity[1,2]. The electrical conductivity can be expressed by $\sigma = ne\mu$, where n is carrier concentration and μ is carrier mobility. Notice that an important factor that affects carrier mobility is the carrier effective mass, which is directly determined by the band structure properties of thermoelectric materials.

Unlike thermoelectric materials such as $(Bi,Sb)_2Te_3$[3,4], $Pb(Te,Se)$[3,4] and SnSe[5] with band edges states consisted of s and p states, there is another class of thermoelectric materials, half-heusler alloys, which have flat band edge states because of the more localized d orbitals of transition metal constituents[6]. The heavy band is not favorable for carrier mobility due to the resulting large effective mass, while it is beneficial to thermopower as discussed in Ref[7]. Half-Heuslers are ternary compounds, ABC (space group $F\bar{4}3m$), which consist of a late transition metal, an early transition metal and one main group element like group IV or V. Here, we only consider the semiconducting half-heusler alloys with 18 valence electrons[8].

Large power factor and low thermal conductivity are essential to high ZT. Half-Heusler (HH) type thermoelectric materials like n-type $ZrNiSn$[9], p-type $ZrCoSb$[10] and p-type $FeNbSb$[11] have attracted particular attention due to their high temperature stability and good thermoelectric performance resulting from high power factor at high temperature[9–15]. The high ZT of 1.5 was reported in p-type $FeNb_{1-x}Hf_xSb$ alloy at 1200 K[12]. The reported power factor ranges from 4.3 to 5.5×10^{-3} $Wm^{-1}K^{-2}$ at p_{opt} of $\sim2\times10^{21}$ cm^{-3} at 800 K for $FeNb_{1-x}Hf_xSb$[12]. This is in contrast to the power factor of only 1.4×10^{-3} $Wm^{-1}K^{-2}$ for p-type SnSe with ZT of 2.0 around 773 K[5]. It is therefore clear that the drawback of HH thermoelectric materials is their high thermal conductivity. For example, for $FeNb_{0.88}Hf_{0.12}Sb$ at 1200 K, the total thermal conductivity is approximately 4 $Wm^{-1}K^{-1}$[12], while for hole-doped SnSe, the total thermal conductivity is about 0.55 $Wm^{-1}K^{-1}$[5]. Therefore, in order to raise ZT of HH compounds higher, it is important to further optimize the properties of HH compounds those already studied or find new HH compounds with lower thermal conductivity and/or higher power factor.

In this work, the electronic properties of half-heusler compound CoVSn are studied within density functional theory, followed by its transport properties by Boltzmann transport theory. The phonon dispersion are also studied by lattice dynamics calculation. The group velocities of acoustical branches for several typical half-heusler thermoelectric materials are calculated. This provides qualitative information regarding the lattice conductivity in relation to CoVSn. We show the potential of CoVSn as a good performance thermoelectric material based on calculated material properties.
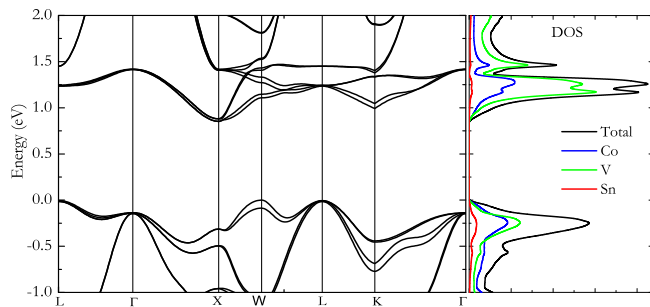
FIG. 1: Calculated band structure together with density of states (DOS) of CoVSn using MBJ with SOC. The Fermi level is set to zero.

II. METHODS

Our electronic structure calculations are performed using the linearized augmented-plane-wave (LAPW) method[16] as implemented in the WIEN2K code[17]. The volume of half-heusler compounds studied here is obtained using the Perdew-Burke-Ernzerhof (PBE) generalized-gradient approximation (GGA)[18]. The optimized lattice constant of 5.828 Å for CoVSn is used in all our calculations except phonon calculation. The band gap is important for thermoelectric properties. We calculate the electronic structure using the modified Becke-Johnson (MBJ) potential[19]. This potential gives improved band gaps for simple semiconductors and insulators as compared to standard density functionals[19,20]. Our transport coefficients are calculated using Boltzmann theory within the constant scattering time approximation (CSTA)[21] as implemented in the BoltzTraP code[22] based on the electronic structure obtained with the MBJ potential. This method has been used successfully to calculate the thermopower of many thermoelectric materials[23,24]. The spin-orbit coupling is considered in current electronic structure and transport calculations. Well converged basis sets defined by a cutoff $RT_{max}=9.0$ for the plane-wave vector plus local orbitals for the semi-core states are used. Here, k_{max} is the plane-wave cutoff, and R is the sphere radius. For Co, Sn and V, the radius are taken as 2.37, 2.37 and 2.31 bohr respectively. A k-point sampling of $8\times8\times8$ is used for total energy calculations. A much denser k-point mesh $48\times48\times48$ is is used for transport calculations and good convergence has been achieved.

III. RESULTS AND DISCUSSION

Our calculated band structure together with the density of states for CoVSn using the MBJ potential is shown in Fig. 1. The states close the valence band edge are mainly contributed by transition metal elements Co and V, and further analysis show that there are mainly d orbitals (not shown here) as discussed before. Between the

energy 0 and -0.25 eV, the density of states increases very quickly, which will lead to large thermopower. As for the band structure, our calculated band gap (W-X) for CoVSn is 0.85 eV. The valence band maximum is at W point, which is only slightly higher than L point about 6 meV. We also notice that the band maxima at Γ and X point is only 0.14 and 0.31 eV lower than that of W point, respectively.

Therefore this compound shows converged bands at the W and L points, which is a feature that has been associated with thermoelectric performance.[25] Furthermore both of these points have degenerate or near degenerate bands at the maximum, which can lead to additional enhancement of the power factor. It also leads to complex shaped bands which is also favorable for thermoelectric performance. These band structure effects - in particular the band *degeneracy*, complex band shapes, and band *convergence* are critical to the transport properties of this material. The conductivity at fixed Seebeck coefficient - a key parameter for a useful thermolectric - is therefore substantially enhanced relative to that of a single isolated parabolic band extremum similar to the certain IV-VI thermoelectric semiconductors with complex electronic structures[26].

The importance of increased band degeneracy is also demonstrated in Bi_2Te_3[27] and $SnSe$[5] systems. Further insight also can be obtained from the isoenergy surface of CoVSn, as presented in Fig. 2. The four isoenergy surfaces in the top panel of Fig. 2 correspond to four bands across the energy of VBM-0.15 eV. The first two isoenergy surfaces with pockets at L point are close to ellipsoids, while the last two have deviations from spherical or ellipsoidal shapes, particularly the last one with obvious corrugated shape[26]. We also notice that at Γ point, the pocket becomes larger and larger and the shape of the pocket becomes more and more complicated. In the bottom panel of Fig. 2, the four isoenergy surfaces corresponding to four bands across the energy of CBM+0.15 eV are shown. The first two pockets have some deviations from spherical or ellipsoidal shapes, while the last two are close to ellipsoids. The thermopower can be enhanced from the deviations of isoenergy surface from spherical or ellipsoidal shapes, and the greater the deviation, the greater the enhancement[27]. Therefore, the better thermopower of p-type than that of n-type doped CoVSn can be expected according to our above discussions and will be confirmed by our thermopower calculations in the following.

The doping dependence of the thermopower is shown for various temperatures in Fig. 3. The thermopower is isotropic since the crystal structure of CoVSn is cubic. For p-type, one notes that the thermopower is better than that of n-type, as a function of carrier concentration for all temperatures. This originates from the band structure difference between the bands near VBM and CBM as depicted in Figs 1 and 2. Both for n- and p-type, for all temperatures, CoVSn display a wide range of carrier concentration where the thermopower
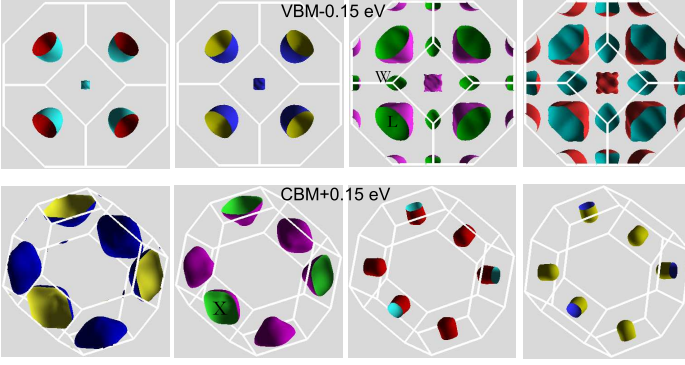
3

FIG. 2: Calculated isoenergy surfaces for CoVSn near VBM and CBM. There are four bands across the energy of VBM-0.15 eV as shown in the top panel, as is CBM+0.15 eV shown in the bottom panel. The high symmetry k points like L, W and X are marked.
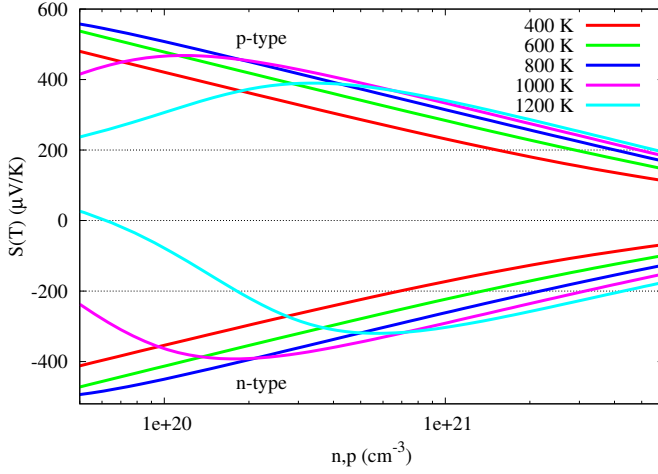

FIG. 4: Calculated thermopower for CoVSn at some fixed concentrations as a function of temperature.

FIG. 3: Calculated Seebeck coefficient as a function of carrier concentration for CoVSn for p-type and n-type doping. The horizontal dashed line indicates a thermopower magnitude of 200 μV/K, generally the minimum necessary for a high-performance thermoelectric.

FIG. 5: Calculated power factor $S^2\sigma/\tau$ for CoVSn and FeNbSb at some fixed temperatures as a function of carrier concentrations.

is large than 200 μV/K. For p-type, at 1000 and 1200 K, the highest thermopower is 470 and 390 μV/K, at concentration of 1.2×10^{20}cm^{-3} and 3.3×10^{20}cm^{-3}, respectively. For n-type, at 1000 and 1200 K, the highest thermopower is -390 and -320 μV/K, at concentration of 1.9×10^{20}cm^{-3} and 5.6×10^{20}cm^{-3}, respectively. Notice that at the same temperature like 1000 or 1200K, the highest thermopower for p-type is higher than that of n-type at a relatively lower carrier concentration. Generally, for most materials, optimum performance typically occurs at carrier concentrations above those where the maximum thermopower occurs. As we mentioned before, for half-heusler alloys, in order to get a high performance thermoelectric, the optimum carrier concentration is around 10^{21}cm^{-3}[12]. One notes that at high temperature 1000 and 1200 K, up to 4×10^{21}cm^{-3}, the thermopower for CoVSn is still higher than 200 μV/K. There
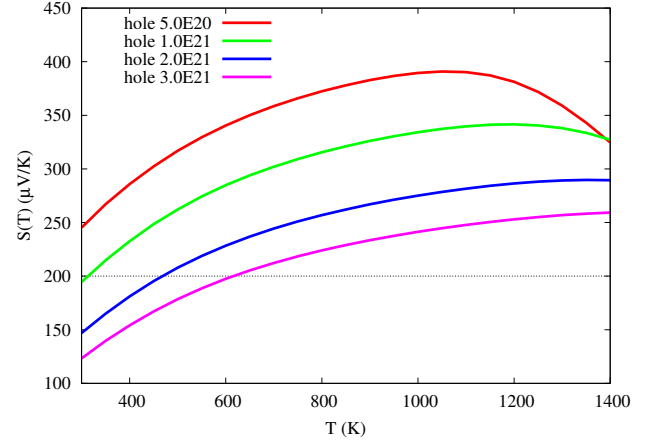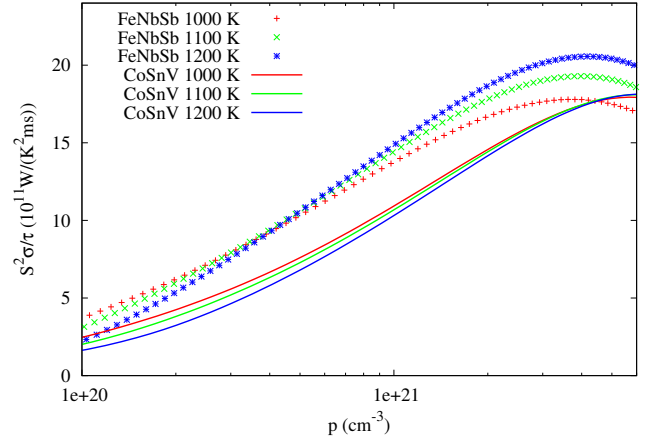
is also clear bipolar effect for both n- and p-type at high temperature, where is well below the optimal carrier concentration regime.

To make the temperature dependence of thermopower more clear, the temperature dependence results at four fixed hole concentrations are present in Fig. 4. For concentrations 5.0×10^{20}cm^{-3} and 1.0×10^{21}cm^{-3}, the highest thermopower are about 390 and 340 μV/K, at temperature 1050 and 1150 K, respectively, while for concentration 2.0×10^{21}cm^{-3} and 3.0×10^{21}cm^{-3}, the thermopowers are approximately 286 and 252 μV/K at 1200 K.

The power factor $S^2\sigma/\tau$ (with respect to an average unknown scattering time) at 1000, 1100 and 1200 K for p-type doping is shown in Fig. 5. Our calculated power factor $S^2\sigma/\tau$ for FeNbSb is also plotted for comparison. The plot depicts comparable behavior for FeNbSb and CoVSn, with a little smaller for the latter. For example, at 1000 K and 1.0×10^{21}, our calculated $S^2\sigma/\tau$ for CoVSn and FeNbSb are 10.5 and 13 (in unit of 10^{11}W/(K^2ms)),
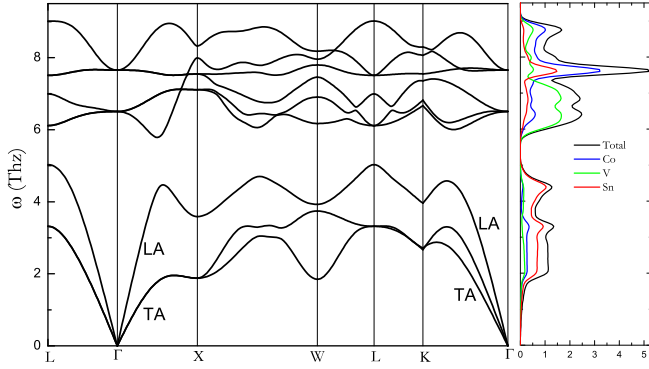
FIG. 6: Calculated phonon dispersion and phonon density of states for CoVSn.

TABLE I: Calculated group velocities of acoustical modes along Γ-X and Γ-L directions. The unit is m/s.

	Γ to X		Γ to L	
	TA	LA	TA	LA
CoVSn	2573	5709	3136	5116
CoSnNb	2847	5813	3330	5277
IrGeNb	3002	4991	2722	5251
FeNbSb	2940	5997	3503	5361
ZrCoSb	2854	5780	3365	5205
ZrNiSn	2868	5516	3150	5200

respectively.

For a good thermoelectric material, the thermal conductivity, especially lattice part k_l, which is determined by the lattice dynamics, must be low. We performed lattice dynamics calculations for CoVSn using the PBE functional[18] for the exchange correlation potential and the projector augmented wave (PAW) method[28] as implemented in the Vienna ab initio simulation package[29]. A $2\times2\times2$ k-point grid in a $3\times3\times3$ supercell containing 81 atoms is used, along with an energy cutoff of 500 eV. The optimized lattice constant is 5.806 Å here for phonon dispersion calculation. Our calculated phonon dispersion together with phonon density of states is shown in Fig. 6. There are three acoustical branches and six optical branches since 3 atoms are in the primitive cell. There is a gap between acoustical and optical modes. For acoustical modes, Sn dominates in the density of states since it is the heaviest element among Co, V and Sn. Co and V contribute most to the optical modes.

Phonon acoustic branches dominate lattice thermal conductivity since they have greater energy dispersion and therefore a broader distribution of phonon velocities, while the optical branches have quite weak energy dispersion and therefore the velocity is low and make small contribution to lattice thermal conductivity[30]. Since low sound speed is important for a reduced k_l, it is natural to search thermoelectric materials with small slope of acoustical modes.

In the following, in order to make a comparison with other good half-heusler thermoelectric alloys like FeNbSb, ZrNiSn and ZrCoSb, the group velocities of acoustic modes are calculated and collected in Table I, which mainly determines the lattice thermal conductivity. Two directions Γ-X ((001)) and Γ-L ((111)) along with transverse acoustical (TA) branch and longitudinal acoustical (LA) branch are considered. Notice that TA branches are degenerate in Γ-X and Γ-L directions. For CoVSn, the TA and LA sound speeds are 2573, 5709, 3136 and 5116 m/s, respectively, along above two directions. FeNbSb, its TA and LA sound speeds are 2940, 5997, 3503 and 5361 m/s, respectively, and for ZrCoSb, its TA and LA sound speeds are 2854, 5780, 3365 and

5205 m/s. Therefore, among CoVSn, FeNbSb and ZrCoSb, CoVSn has the smallest acoustic speeds. Based on our above discussions, compared to FeNbSb and ZrCoSb, the conclusion that CoVSn material has good potential for lowering thermal conductivity relative to the other compounds since its sound speeds are smallest. This is in accord with direct lattice thermal conductivity calculations[31]. Notice that Bi_2Te_3 has smaller lattice thermal conductivity, which is in consistent with its corresponding smaller sound speeds, compared to above half-heusler alloys. For Bi_2Te_3, along Γ-L direction, the sound speeds of TA and LA are 1395, 1728, and 2394 m/s, respectively, and along Γ-Z direction, the speeds are 1774 and 1811 m/s[27].

Experimentally Lue et $al.$ has shown that CoVSn can be produced, at least with partial atomic ordering on the half-Heusler lattice. They successfully prepared CoVSn in an RF induction furnace from elemental ingredients, while attempts by arc melting method were not successful[32]. Another study of $Ti_{1-x}V_xCoSb_{1-x}Sn_x$ found that x cannot be increased beyond 0.4, which indicates that CoVSn cannot be synthesized by conventional solid-state reaction[33]. Theoretically Carrete et $al.$ predicted CoVSn is both thermally and mechanically stable[31] while Zakutayev et $al.$ predict CoVSn is not stable theoretically[34], based on calculations using the fitted elemental-phase reference energies method[35]. In a very recent work, Ma et $al.$ reported that almost all the experimentally synthesized half-Heusler compounds lie on or close to the convex hull, with hull distances between 0.0 and about 0.1 eV/atom. They selected 110 compounds (experimentally reported and unreported), in which they find that (shown Fig. 6 in Ref.[36]) that the vast majority of the reported half-Heusler compounds that have been experimentally synthesized lie on or close to the calculated convex hull-37 compounds are on the convex hull ($i.e.$, a hull distance of 0 eV/atom) and an additional 52 lie relatively close to it ($i.e.$, a hull distance less than about 0.1 eV/atom)[36]. They predicted that CoVSn is in the half-heusler structure because its hull distance is only 0.012 eV/atom just above the convex hull[36]. We also did stability calculations considering competing phases. Our total energy calculations for the competing phases show that CoVSn is thermodynamically stable with the PBE
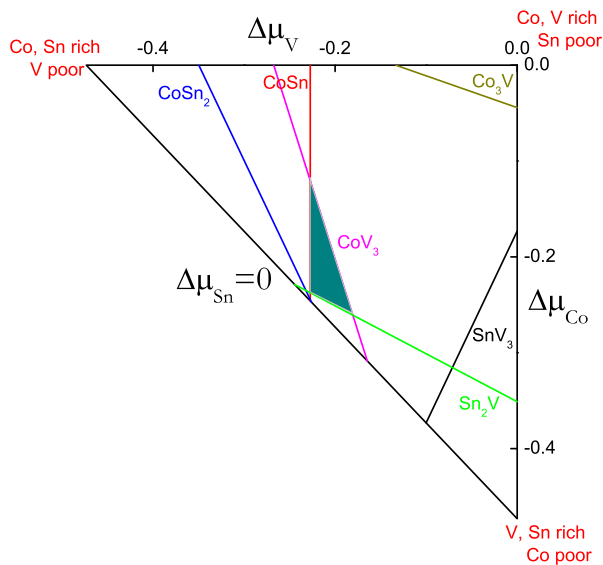
FIG. 7: Calculated phase diagram for CoVSn. The stable region for CoVSn is shaded. The unit for chemical potentials $\Delta\mu_{Co}$ and $\Delta\mu_V$ is eV.

functional, which is shown in the shaded region in Fig. 7. With careful control of growth conditions (which affects the elemental chemical potentials $\Delta\mu$), the synthesis of the single-phase CoVSn is possible. According to above discussions, the method and condition that used in the synthesis of CoVSn should be carefully controlled. In any case it may be that CoVSn can be synthesized by non-equilibrium ways, e.g. quenching via melt spinning or in

thin film deposition. Melt spinning is a method that was used for other nanostructured thermoelectrics[37,38].

IV. SUMMARY

The electronic structure and potential thermoelectric performance of half-heusler alloy CoVSn are investigated theoretically. A large thermopower is obtained for CoVSn, particularly for the *p*-type doping. This originates from several close valence band maxima and corrugated shape in the isoenergy surface according to our calculations. This type of complex band shape and degeneracy enables resolution of the conundrum posed by normally contradictory requirements of high thermopower and high conductivity needed to obtain high ZT. Our calculated power factor $S^2\sigma/\tau$ for CoVSn can be comparable to that of FeNbSb at the optimal carrier concentration. A smaller group velocities of acoustical modes for CoVSn indicates that the possibility of smaller lattice thermal conductivity, which also good for the overall thermoelectric performance.

Acknowledgments

[1] C. Wood, Materials for thermoelectric energy conversion, Rep. Prog. Phys. 51, 459 (1988).

[2] J. Yang, L. Xi, W. Qiu, L. Wu, X. Shi, L. Chen, J. Yang, W. Zhang, C. Uher and D.J. Singh, npj Computational Materials 2, 15015 (2016).

[3] A. F. Ioffe, Semiconductor Thermoelements and Thermoelectric Cooling (Inforsearch, London, 1957).

[4] D. M. Rowe, CRC Handbook of Thermoelectrics (CRC Press, New York, 1995).

[5] L. D. Zhao, G. J. Tan, S. Q. Hao, J. Q. He, Y. L. Pei, H. Chi, H. Wang, S. K. Gong, H. B. Xu, V. P. Dravid, C. Uher, G. J. Snyder, C. Wolverton, and M. G. Kanatzidis, Ultrahigh power factor and thermoelectric performance in hole-doped single-crystal SnSe, Science 351, 141 (2016).

[6] C. Uher, J. Yang, S. Hu, D. T. Morelli, and G. P. Meisner, Transport properties of pure and doped MNiSn (M=Zr, Hf), Phys. Rev. B 59, 8615 (1999).

[7] K. Kuroki and R. Arita, Pudding mold band drives large thermopower in $Na_x CoO_2$, J. Phys. Soc. Jpn. 76, 083707 (2007).

[8] D Jung, H.-J Koo, M.-H Whangbo, Study of the 18-electron band gap and ferromagnetism in semi-Heusler compounds by non-spin-polarized electronic band structure calculations, J. Mol. Struct.Theochem 527, 113 (2000).

[9] C. Yua, T.-J. Zhu, R.-Z. Shi, Y. Zhang, X.-B. Zhao, J. He, High-performance half-Heusler thermoelectric materials $Hf_{1-x}Zr_xNiSn_{1-y}Sb_y$ prepared by levitation melting and spark plasma sintering, Acta Mater. 57, 2757 (2009).

[10] S. R. Culp, J. W. Simonson, S. J. Poon, V. Ponnambalam, J. Edwards, and T. M. Tritt, (Zr,Hf)Co(Sb,Sn) half-Heusler phases as high-temperature (>700 °C) *p*-type thermoelectric materials, Appl. Phys. Lett. 93, 022105 (2008).

[11] C. Fu, T. Zhu, Y. Liu, H. Xie and X. Zhao,Band engineering of high performance *p*-type FeNbSb based half-Heusler thermoelectric materials for figure of merit zT>1,Energy Environ. Sci.,8, 216 (2015).

[12] C. Fu, S. Bai, Y. Liu, Y. Tang, L. Chen, X. Zhao, T. Zhu, Realizing high figure of merit in heavy-band *p*-type half-Heusler thermoelectric materials. Nat. Commun. 6, 8144 (2015).

[13] L. Chen, S. Gao, X. Zeng, A. Mehdizadeh Dehkordi, T. M. Tritt, and S. J. Poon, Uncovering high thermoelectric figure of merit in (Hf,Zr)NiSn half-Heusler alloys, Appl. Phys. Lett. 107, 041902 (2015).

[14] R. He, L. Huang, Y. Wang, G. Samsonidze, B. Kozinsky, Q. Zhang, and Z. Ren, Enhanced thermoelectric properties of *n*-type NbCoSn half-Heusler by improving phase purity, APL Mater. 4, 104804 (2016).

[15] G. Fiedler and P. Kratzer, Ternary semiconductors NiZrSn and CoZrBi with half-Heusler structure: A first-principles study, Phys. Rev. B 94, 075203 (2016).

[16] D. J. Singh and L. Nordstrom, Planewaves Pseudopotentials and the LAPW Method, 2nd ed. (Springer, Berlin, 2006).

[17] P. Blaha, K. Schwarz, G. Madsen, D. Kvasnicka, and J. Luitz, WIEN2k, An Augmented Plane Wave+Local Orbitals Program for Calculating Crystal Properties (K. Schwarz, Tech. Univ. Wien, Austria, 2001).

[18] J. P. Perdew, K. Burke, and M. Ernzerhof, Generalized Gradient Approximation Made Simple, Phys. Rev. Lett. 77, 3865 (1996).

[19] F. Tran and P. Blaha, Accurate band gaps of semiconductors and insulators with a semilocal exchange-correlation potential, Phys. Rev. Lett. 102, 226401 (2009).

[20] D. Koller, F. Tran, and P. Blaha, Merits and limits of the modified Becke-Johnson exchange potential, Phys. Rev. B 83, 195134 (2011).

[21] D. Parker and D. J. Singh, High-temperature thermoelectric performance of heavily doped PbSe, Phys. Rev. B 82, 035204 (2010).

[22] G. K. H. Madsen and D. J. Singh, Boltztrap. A code for calculating band-structure dependent quantities, Comput. Phys. Commun. 175, 67 (2006).

[23] D. J. Singh, Electronic and thermoelectric properties of $CuCoO_2$: Density functional calculations, Phys. Rev. B 76, 085110 (2007).

[24] D. Parker and D. J. Singh, Potential Thermoelectric Performance from Optimization of Hole-Doped Bi_2Se_3, Phys. Rev. X 1, 021005 (2011).

[25] Y. Pei, X. Shi, A. LaLonde, H. Wang, L. Chen, L. and G.J. Snyder, G.J. Convergence of electronic bands for high performance bulk thermoelectrics. Nature, **473**, 66 (2011).

[26] X. Chen, D. Parker, and D. J. Singh, Importance of nonparabolic band effects in the thermoelectric properties of semiconductors, Sci. Rep. **3**, 3168 (2013).

[27] H. Shi, D. Parker, M.-H. Du, and D.J. Singh, Connecting Thermoelectric Performance and Topological-Insulator Behavior: Bi2Te3 and Bi2Te2Se from First Principles, Phys. Rev. Appl. 3, 014004 (2015).

[28] G. Kresse and D. Joubert, Phys. Rev. B 59, 1758 (1999).

[29] G. Kresse and J. Furthmuller, Phys. Rev. B 54, 11169 (1996).

[30] P. Pichanusakorn and P. Bandaru, Nanostructured thermoelectrics, Mater. Sci. Eng. R-Rep. 67, 19 (2010).

[31] J. Carrete, W. Li, N. Mingo, S. Wang, and S. Curtarolo, Finding Unprecedentedly Low-Thermal-Conductivity Half-Heusler Semiconductors via High-Throughput Materials Modeling, Phys. Rev. X 4, 011019 (2014).

[32] C.S. Lue, Y. Oner, D.G. Naugle, J.H. Ross, Magnetism of new semi-Heusler compounds FeVSn and CoVSn, IEEE Trans. Magn. 37, 2138 (2001).

[33] M. Asaad, J. Buckman, R. I. Smithc, and J. Bos, Thermoelectric properties and high-temperature stability of the $Ti_{1-x}V_xCoSb_{1-x}Sn_x$ half-Heusler alloys, RSC Adv. 6, 56511 (2016).

[34] A. Zakutayev, X. Zhang, A. Nagaraja, L. Yu, S. Lany, T. Mason, D. S. Ginley, and A. Zunger, Theoretical Prediction and Experimental Realization of New Stable Inorganic Materials Using the Inverse Design Approach, J. Am. Chem. Soc. 135, 10048 (2013).

[35] V. Stevanovi*c*, S. Lany, X. Zhang and A. Zunger, Correcting density functional theory for accurate predictions of compound enthalpies of formation: Fitted elemental-phase reference energies, Phys. Rev. B 85, 115104 (2012).

[36] J. Ma, V. I. Hegde, K. Munira, Y. Xie, S. Keshavarz, D. T. Mildebrath, C. Wolverton, A. W. Ghosh, and W. H. Butler, Computational investigation of half-Heusler compounds for spintronics applications, Phys. Rev. B 95, 024411 (2017).

[37] W. Xie, X. Tang, Y. Yan, Q. Zhang, and T. Tritt, Unique nanostructures and enhanced thermoelectric performance of melt-spun BiSbTe alloys, Appl. Phys. Lett. 94 102111 (2009).

[38] G. Tan, W. Liu, S.Wang, Y. Yan, H. Li, X. Tang, and C. Uher, Rapid preparation of $CeFe_4Sb_{12}$ skutterudite by melt spinning: rich nanostructures and high thermoelectric performance, J. Mater. Chem. A 1, 12657 (2013).